

Vacuum Brazing of WC-8Co Cemented Carbides to Carbon Steel Using Pure Cu and Ag-28Cu as Filler Metal

X.Z. Zhang, G.W. Liu, J.N. Tao, H.C. Shao, H. Fu, T.Z. Pan, and G.J. Qiao

(Submitted May 30, 2016; in revised form October 18, 2016; published online December 9, 2016)

The wetting and spreading behavior of commercial pure Cu and Ag-28Cu alloy on WC-8Co cemented carbide were investigated by the sessile drop technique. The contact angle of both systems obviously decreases with moderately increasing the wetting temperature. Vacuum brazing of the WC-8Co cemented carbide to SAE1045 steel using the pure Cu or Ag-28Cu as filler metal was further carried out based on the wetting results. The interfacial interactions and joint mechanical behavior involving microhardness, shear strength and fracture were analyzed and discussed. An obvious Fe-Cu-Co transition layer is detected at the WC-8Co/Cu interface, while no obvious reaction layer is observed at the whole WC-8Co/Ag-28Cu/SAE1045 brazing seam. The microhardness values of the two interlayers and the steel substrate near the two interlayers increase more or less, while those of WC-8Co cemented carbide substrates adjacent to the two interlayers decrease. The WC-8Co/SAE1045 joints using pure Cu and Ag-28Cu alloy as filler metals obtain average shear strength values of about 172 and 136 MPa, and both of the joint fractures occur in the interlayers.

Keywords cemented carbide, interface, joining, mechanical property, steel, wetting

1. Introduction

Tungsten carbide/cobalt (WC-Co) cemented carbides, consisting of large volume fractions of WC particles embedded in the soft and ductile Co binder, can serve as hard and tough tool material (Ref 1). Due to the good compatibility of the hard WC grains and the ductile Co binder phase, the WC-Co cemented carbides show high hardness, strength, refractoriness, as well as compressive deformation and wear resistances. These good mechanical properties make the WC-Co cemented carbides be typically used as drilling or cutting tools, structural components, mining bits and press molds, as well as miniature drills for highly integrated printed circuit boards or rock drills (Ref 2–5). However, the widespread use of cemented carbides is limited by their expensive cost and brittleness. The joining of cemented carbides to structural steel has received much attention in recent years because of the compensatory properties. Presently, their joining techniques are mainly composed of brazing (Ref 6–13), diffusion bonding (Ref 14–16), fusion welding (Ref 17, 18) and partial transient liquid-phase bonding (Ref 19), among which brazing is an appropriate process to join

cemented carbides to steel in terms of simple process and low cost.

As we know, wettability as manifest in the contact angle, θ , has long been recognized as a critical parameter in determining the brazability of material by a molten filler metal. However, the related research besides Akbari Mousavi's investigation (Ref 9) on wetting of cemented carbides by metals was rare, though the wetting of molten Zr-base metallic glass-forming alloy (Ref 20) and Zr₂Cu alloy (Ref 21) on dense polycrystalline WC was investigated. Akbari Mousavi et al. (Ref 9) investigated the wettability of Ag-Cd alloys on cemented carbide and obtained the final contact angles of less than 10° at 870 and 850 °C for 20 min. Meanwhile, in order to achieve high-performance brazed joints, the filler metals used to braze the cemented carbides to steel were mainly focus on the Cu- and Ag-based alloys due to their excellent ductility and toughness, such as Cu-Zn (Ref 6), Cu-Zn-Ni (Ref 7), Cu-Sn-Ni (Ref 8), Ag-Cd (Ref 9) and Ag-Cu-Zn-(Mn, Ni, Co) (Ref 10, 11). In addition, Lee et al. (Ref 12, 13) reported that the WC-Co cemented carbide was successfully brazed with carbon steel using multiple layers of Cu and Ni alloys as insert metal. In the present study, the wetting and spreading behavior of commercial pure Cu and Ag-28Cu eutectic alloy on the WC-8Co cemented carbide at different temperatures were addressed, and the brazing of WC-8Co cemented carbide to SAE1045 carbon steel was carried out based on the wetting results. Furthermore, the interfacial interactions and joint mechanical behavior involving microhardness, shear strength and fracture were investigated.

2. Experimental

The commercial WC-8Co (all compositions are given in wt.%) cemented carbides with dimensions of Ø 20 mm × 6 mm (Zhuzhou Weiye Carbide Industrial Co., Ltd, Zhuzhou, China) and SAE1045 carbon steel with dimen-

X.Z. Zhang, J.N. Tao, H.C. Shao, and H. Fu, School of Materials Science and Engineering, Jiangsu University, Zhenjiang 212013, China; G.W. Liu, School of Materials Science and Engineering, Jiangsu University, Zhenjiang 212013, China; and Suzhou Pant Piezoelectric Tech Co. Ltd., Suzhou 215300, China; T.Z. Pan, Suzhou Pant Piezoelectric Tech Co. Ltd., Suzhou 215300, China; and G.J. Qiao, School of Materials Science and Engineering, Jiangsu University, Zhenjiang 212013, China; and State Key Laboratory for Mechanical Behavior of Materials, Xi'an Jiaotong University, Xi'an 710049, China. Contact e-mails: gwliu76@ujs.edu.cn and gjqiao@ujs.edu.cn.

sions of $\text{Ø } 15 \text{ mm} \times 5 \text{ mm}$ were used as the substrates for wetting and/or brazing experiments. The wetting and brazing surfaces of the cemented carbide and SAE1045 carbon steel pieces were ground to a plane by automatic grinding machine using the sequence 400, 800 and 1200 mesh diamond grinding plates, and further polished using diamond grains of $1 \mu\text{m}$ until a mirror face was obtained. The commercial pure Cu and Ag-28Cu eutectic alloy for the wetting and vacuum brazing experiments were cut from Cu wires of $\text{Ø } 2 \text{ mm}$ (99.9 wt.% purity, Sinopharm Chemical Reagent Co., Ltd.) and Ag-28Cu eutectic alloy filament of $\text{Ø } 0.8 \text{ mm}$ (Northwest Institute for Nonferrous Metal Research, Xi'an, China), respectively.

Before the wetting and joining experiments, all the substrates were given a final ultrasonic cleaning in alcohol. The spherical and annular of Cu and Ag-28Cu alloy were chemically and ultrasonically cleaned and then dried. The wetting and spreading were evaluated by a high-temperature contact angle measuring instrument (OCA15LHT-SV, Dataphysics, Germany), and the heating rate was $5 \text{ }^\circ\text{C}/\text{min}$. Sessile drop tests of pure Cu or Ag-28Cu alloy on the WC-8Co cemented carbide were performed at different temperatures under a high vacuum of $\sim 5 \times 10^{-4} \text{ Pa}$. For the joining process, the WC-8Co, annular Cu or Ag-28Cu filaments and SAE1045 carbon steel were assembled in a graphite mold and finally brazed in a vacuum furnace (vacuity: $\sim 7 \times 10^{-3} \text{ Pa}$, furnace model: High-multi 5000, Japan). A pressure of 10 kPa was applied to the top of the WC-8Co/SAE1045 carbon steel couples. The joining process cycles began at a heating rate of $10 \text{ }^\circ\text{C}/\text{min}$ to $800 \text{ }^\circ\text{C}$ and followed by a heating rate of $5 \text{ }^\circ\text{C}/\text{min}$ up to the bonding temperature (1100 or $850 \text{ }^\circ\text{C}$) for holding 10 min. Finally, the joints were cooled in furnace till $300 \text{ }^\circ\text{C}$ at an average rate of $3 \text{ }^\circ\text{C}/\text{min}$ and then furnace cooled.

After these experiments, the brazed joints were cross-sectioned, polished and then observed to investigate the interfacial behavior by SEM (SU3500, Hitachi) coupled with energy-dispersive spectroscopy (EDS, Model Oxford INCA, Britain). The microhardness of the joints was determined by a HVS-1000 digital microhardness tester. The joint strength was tested by shear-load method using a DDL100 testing machine at the loading speed of $0.5 \text{ mm}/\text{min}$. The mean value of joint strength under each brazing condition was the arithmetical average of three joint samples. The shear test experiments were performed on the specimens according to the literature reported

(Ref 22). Phase compositions of the fracture surfaces of brazed joints were identified by x-ray diffraction (D/max2500PC, Rigaku Corporation) analysis.

3. Results and Discussion

3.1 Wetting and Spreading Behavior

Figure 1 shows the spreading curves of molten Cu and Ag-28Cu alloy on the WC-8Co substrate at the different temperatures and the photographs of solidified drops formed at the final states. As shown in Fig. 1(a), both the molten Cu/WC-8Co systems at 1090 and $1100 \text{ }^\circ\text{C}$ almost reach the equilibrium after $\sim 10 \text{ min}$. The two wetting systems have an identical initial contact angle of $\sim 36^\circ$ due to the same starting melting temperature. Moreover, the initial spreading rate increases from $\sim 4.5 \times 10^{-2}$ to $7.2 \times 10^{-2} \text{ }^\circ/\text{s}$ and the equilibrium contact angle decreases from $\sim 15^\circ$ to 4° with the temperature increasing from 1090 to $1100 \text{ }^\circ\text{C}$. As shown in the Cu-Co binary phase diagram (Fig. 2a) (Ref 23), the molten Cu can react with the Co from the WC-8Co substrate to form the Cu(Co) or Co(Cu) solid solution. As a result, the solid-liquid surface energy (σ_{SL}) of Cu/WC-8Co system should be decreased due to the fact that the interactions between the molten Cu and the WC-8Co substrate increase with the increase in temperature. Thus, referring to the Young's equation ($\cos\theta = (\sigma_{SV} - \sigma_{SL})/\sigma_{LV}$), the numerator ($\sigma_{SV} - \sigma_{SL}$) is increased, while the denominator σ_{LV} can be considered almost invariant, and the contact angle θ is expected to decrease significantly.

As can be seen from the Ag-28Cu/WC-8Co wetting system, two main stages are separated in the contact angle curves. At the beginning of the spreading stage, the spreading of molten Ag-28Cu alloy on the WC-8Co substrate system is much slower than that of the Cu/WC-8Co system. However, during the second stage, the contact angle still decreases gradually with the time going on. Moreover, the spreading cannot reach the equilibrium after 60 min since the Ag-28Cu alloy begins to melt, and the final contact angles at 830 and $850 \text{ }^\circ\text{C}$ are 37.2° and 24.3° , respectively. At the two wetting temperatures, the activity of Ag and Cu atoms is reduced compared to that of Cu atom in the Cu/WC-8Co system at $\sim 1100 \text{ }^\circ\text{C}$ and the formation of Ag(Co) and Cu(Co) solid solution is quite hard, as shown in the Co-Ag and Co-Cu phase diagrams (Fig. 2) (Ref 23).

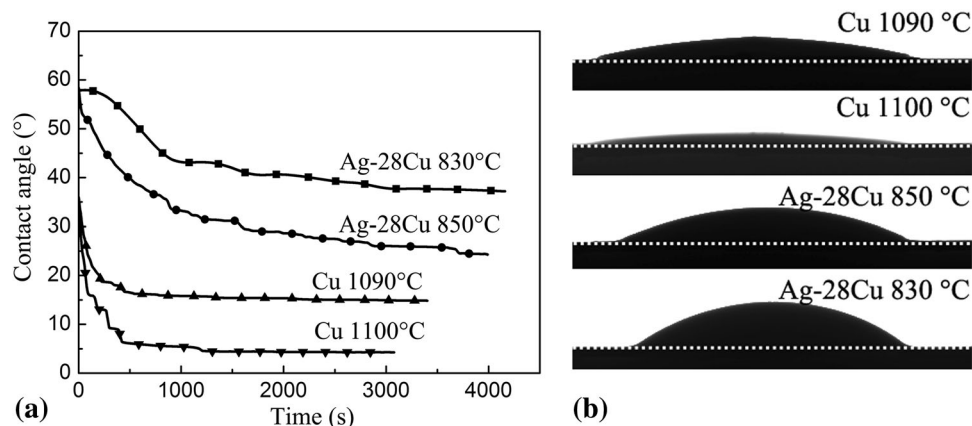


Fig. 1 (a) Spreading curves of molten Cu and Ag-28Cu alloy on the WC-8Co substrate at different temperatures and (b) photographs of solidified drops formed at the final states

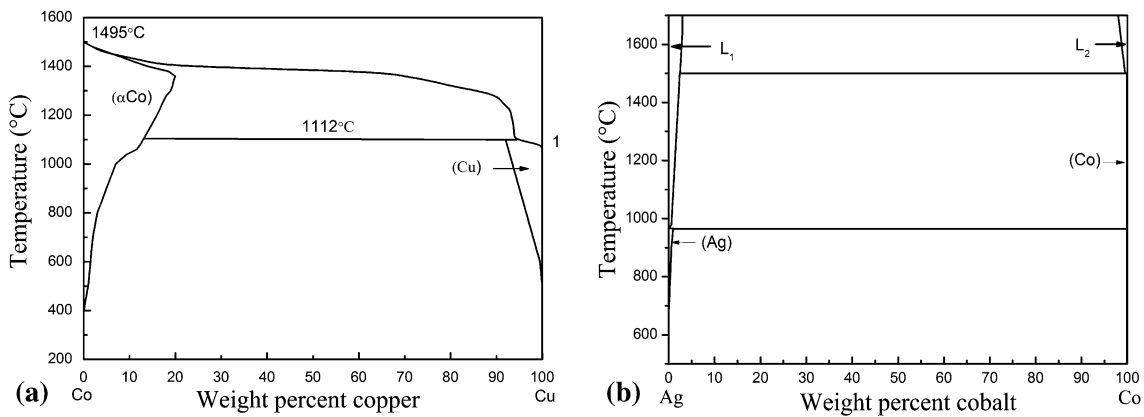


Fig. 2 Phase diagrams of (a) Cu-Co and (b) Ag-Co (Ref 23)

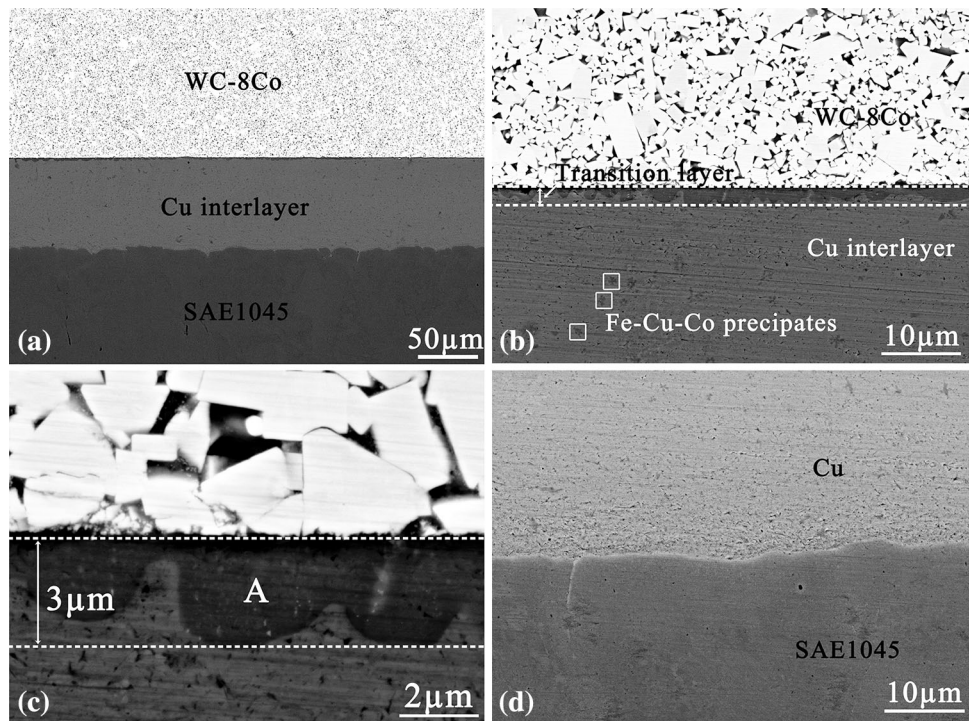


Fig. 3 BSE images of (a) the cross-sectional WC-8Co/Cu/SAE1045 joint brazed at 1100 °C for 10 min, (b, c) the WC-8Co/Cu interface and (d) the Cu/SAE1045 interface

As discussed above, the final contact angles of the two wetting systems decrease significantly when the test temperatures increase from 830 to 850 °C and 1090 to 1100 °C, respectively. Meanwhile, the spreading of Cu/WC-8Co system at 1100 °C after 10 min reaches equilibrium and the contact angle is almost invariant, while for the Ag-28Cu/WC-8Co system at 850 °C after 10 min, the first stage of the spreading curve is basically finished and then the contact angle alters slowly with the time going on. Thus, brazing of the cemented carbides can be carried out under the guidance of the wetting results.

3.2 WC-8Co/SAE1045 Brazed Joints

The WC-8Co cemented carbide was brazed to the SAE1045 steel in a vacuum at 1100 and 850 °C for 10 min using pure Cu

and Ag-28Cu alloy as filler metal, respectively. Figure 3 shows the cross-sectional BSE images of the WC-8Co/Cu/SAE1045 joint. It is clear that a good bonding without obvious defects is obtained in the joint. A transition layer of 2-3 μm is observed at the WC-8Co/Cu interface (Fig. 3c). As confirmed by the elemental EDS profiles of the brazed joint (Fig. 4), the Cu and Fe can diffuse into the WC-8Co substrate for a certain distance, and Co and Fe can also enter into the Cu interlayer to form a Fe- and Co-rich layer (i.e., the transition layer) adjacent to the WC-8Co/Cu interface. The chemical composition (at.%) of the transition layer is 46.2Fe + 45.82Co + 7.98Cu as confirmed by the EDS analysis (point A in Fig. 3c). The transition layer is mainly composed of α-(Fe) and Cu(Co) solid solutions since no binary or ternary compounds exist in the Fe-Cu-Co system (Ref 24, 25). And some precipitates containing Fe, Cu and Co can be

found in the interlayer due to the interdiffusion of these elements. Meanwhile, the W element is not detected in the Cu interlayer due to the fact that the WC particles cannot react with the liquid Cu. In fact, the presence of solid solutions in the transition layer can contribute to obtain a good bonding at the WC-8Co/Cu interface. Moreover, no obvious transition layer forms at the Cu/SAE1045 interface (Fig. 3d), and the Co can diffuse across the Cu interlayer into the SAE1045 substrate to form a thin solid solution layer (γ -Fe(Co)) at the Cu/SAE1045 interface (Fig. 4), which is in accordance with the solid solution concentration in Fe-Co phase diagram at 1100 °C (Ref 23).

Figure 5 shows the cross-sectional BSE images of the WC-8Co/Ag-28Cu/SAE1045 joint brazed at 850 °C for 10 min. The Ag-28Cu filler metal can adhere tightly to the WC-8Co substrate, leaving a smooth and clean interface (Fig. 5b). Two kinds of alternating phases present in the brazing seam, where the dark and white ones are Cu(Ag) and Ag(Cu) solid solutions, respectively. As shown in the elemental EDS profiles of WC-8Co/Ag-28Cu/SAE1045 joint (Fig. 6), the Ag and Cu elements from the filler metal cannot diffuse into the WC-8Co substrate in spite of large elemental concentration gradients at the interface. This is closely related to the formation ability of Co(Ag) and Co(Cu) solid solutions at 850 °C and with the relatively low concentration and activity of Cu in the Ag-28Cu alloy compared to those in the pure Cu. Moreover, the Co and

Fe derived from the two substrates hardly retain in the Ag-28Cu filler metal, which is somewhat different from the Cu/WC-8Co system. This phenomenon may be mainly attributed to the reduced activity of Ag and Cu atoms and the relatively low concentration of Cu in the Ag-28Cu alloy, as well as the relatively low brazing temperature (850 °C). However, a considerable amount of Co diffuses across the Ag-28Cu interlayer into the SAE1045 steel substrate for a long distance, as shown in Fig. 6. Thus, it can be inferred that the Ag-28Cu alloy can serve as a barrier to prevent the Fe to diffuse into the WC-8Co substrate, and as a channel to let the Co enter into the steel substrate.

Hardness profile is a good indicator of the joint microstructure and mechanical behavior. Figure 7 shows the variations of the Vickers microhardness values across the two brazed joints corresponding to Fig. 3(a) and 5(a). As shown in Fig. 7(a), the mean microhardness value in the steel near the SAE1045/Cu interface increases from \sim 295 to 356 HV due to the relatively serious diffusion of Co into the steel. This fact justifies an increase in the microhardness in the brazing seam compared with that of pure Cu, reaching \sim 200 HV, due to the diffusion of the Fe and Co elements from the two substrates into the Cu interlayer during brazing. In addition, in the WC-8Co substrate

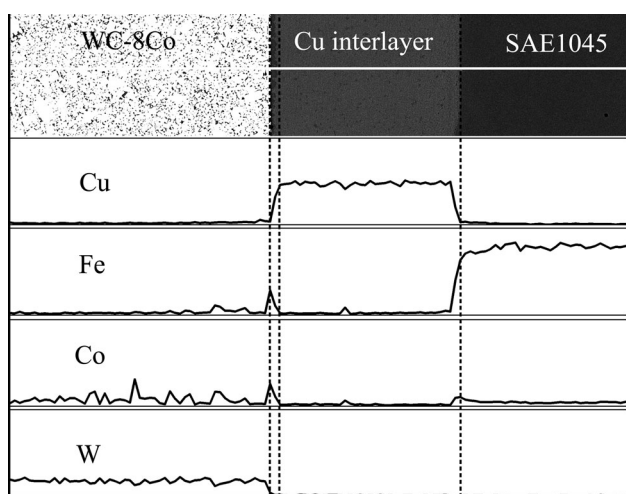


Fig. 4 Elemental EDS profiles across the whole WC-8Co/Cu/SAE1045 brazing area

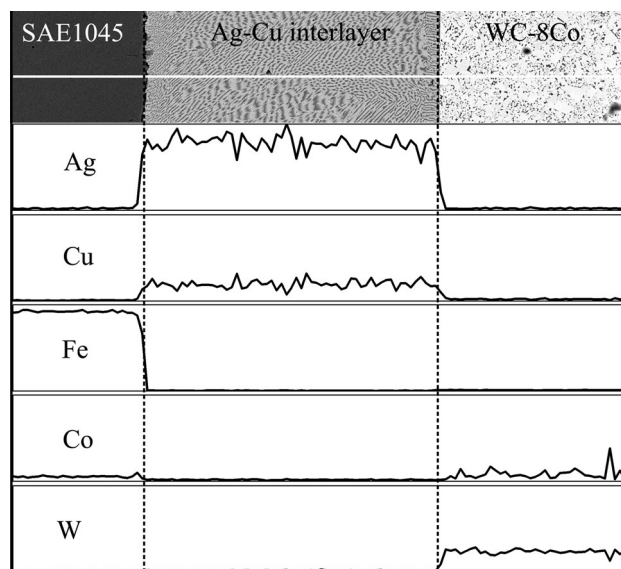


Fig. 6 Elemental EDS profiles across the whole WC-8Co/Ag-28Cu/SAE1045 brazing area

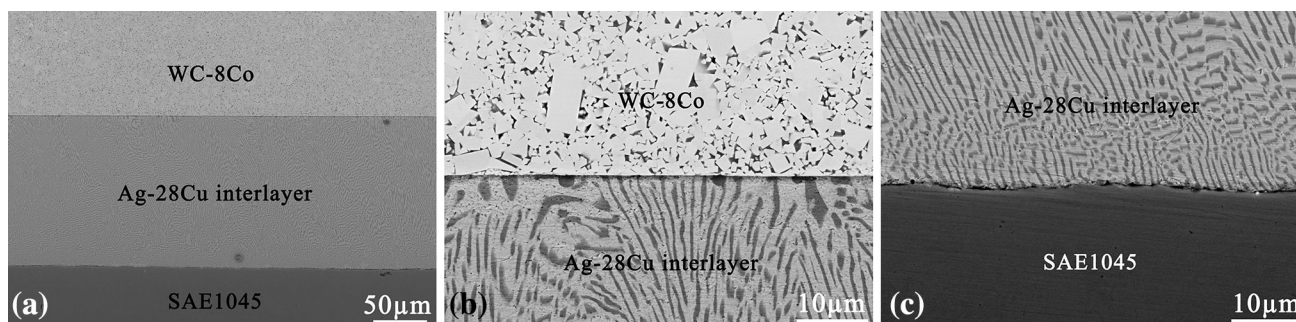


Fig. 5 BSE images of (a) the cross-sectional WC-8Co/Ag-28Cu/SAE1045 joint brazed at 850 °C for 10 min, (b) the WC-8Co/Ag-28Cu interface and (c) the Ag-28Cu/SAE1045 interface

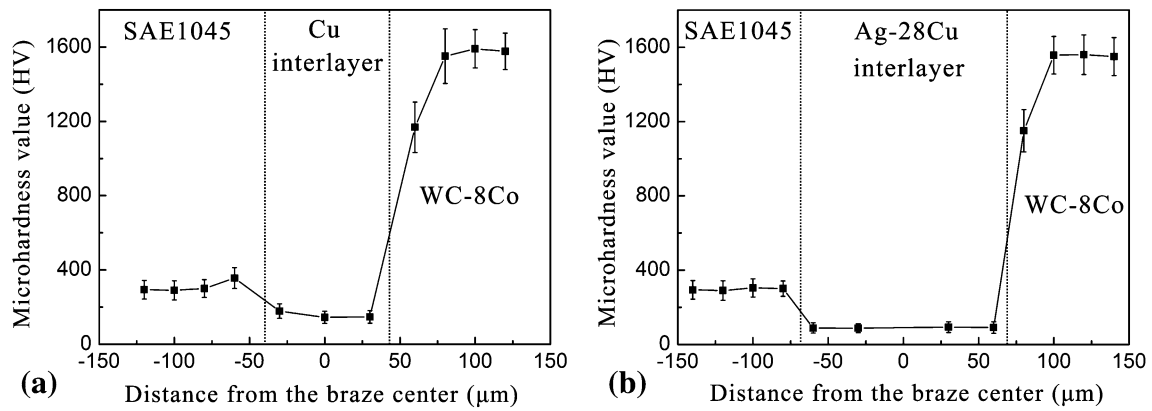


Fig. 7 Microhardness distribution of joint sections of (a) WC-8Co/Cu/SAE1045 and (b) WC-8Co/Ag-28Cu/SAE1045

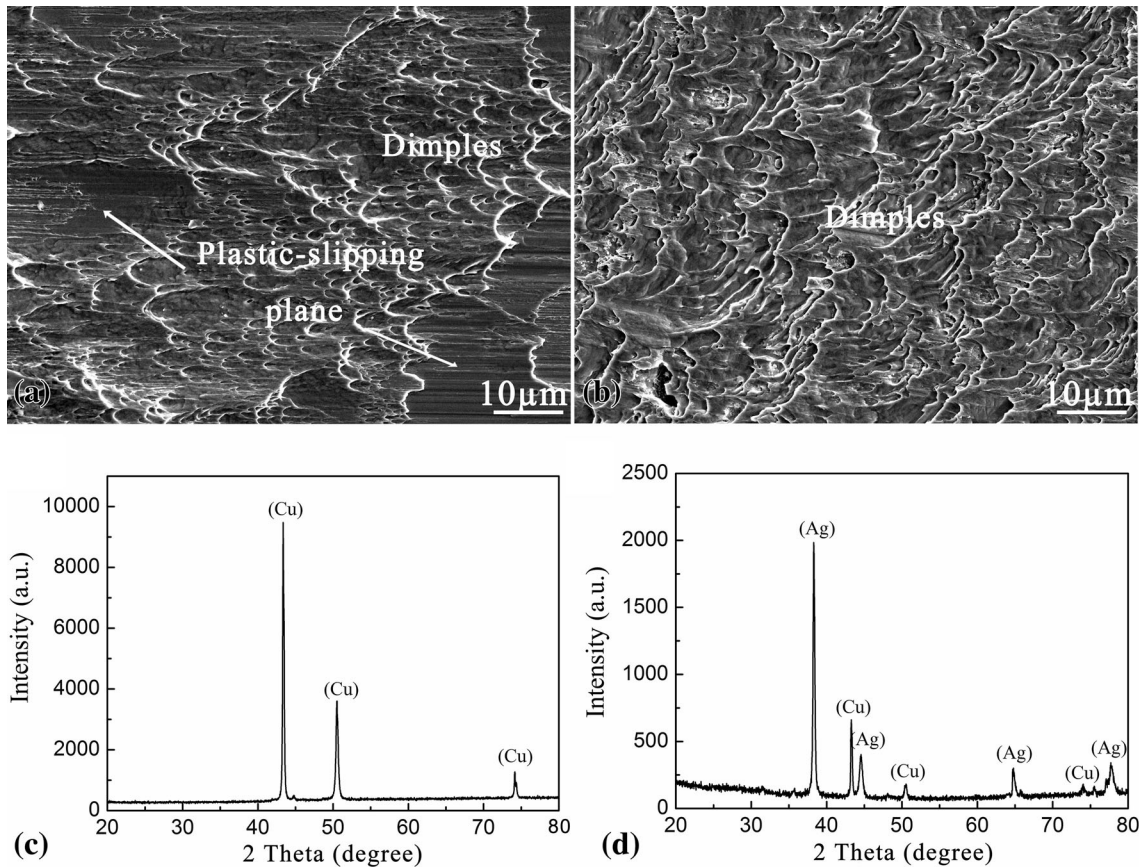


Fig. 8 Typical fracture surface morphologies of the two kinds of WC-8Co/SAE1045 brazed joints and XRD patterns of the two fracture surfaces: (a, c) WC-8Co/Cu/SAE1045, (b, d) WC-8Co/Ag-28Cu/SAE1045

adjacent to the WC-8Co/Cu interface, the mean microhardness decreases to ~ 1168 HV compared to that of the WC-8Co substrate (~ 1550 HV), which can be attributed to the decomposition of the WC-8Co due to the escape of the Co. For the microhardness of the WC-8Co/Ag-28Cu/SAE1045 system (Fig. 7b), no obvious fluctuation of hardness in the SAE1045 substrate is observed although the Co can diffuse across the filler metal into the steel substrate. Similarly, the decrease in microhardness in the WC-8Co substrate adjacent to the WC-8Co/interlayer interface and the increase in microhardness of interlayer are also detected. The microhardness evaluation of the brazed joints shows that the variations of

microhardness in the different zones are associated with the mutual interactions of the metal elements (such as diffusion, solid solution) during brazing.

The Fe from the steel substrate can diffuse across the interlayer into the WC-Co cemented carbide, which are detrimental to the toughness of the joint based on the work reported before (Ref 26). The fracture of WC-8Co/SAE1045 joints may occur along the WC-8Co/filler metal interface due to the diffusion of Fe into the cemented carbide and the decomposition of the WC-8Co cemented carbide. However, both the fractures of the two kinds of WC-8Co/SAE1045 brazed joints occur in the brazing beam, as shown in Fig. 8. In

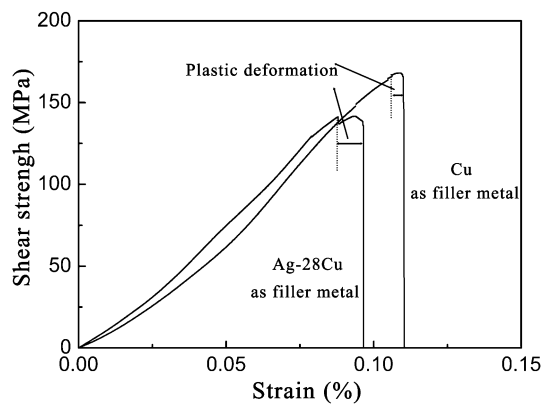


Fig. 9 Typical shear stress-strain curves of the two kinds of WC-8Co/SAE1045 brazed joints

particular, the fractographs of the two kinds of brazed joints are similar, and no WC particles are observed at the two fracture surfaces. Moreover, for the WC-8Co/Cu/SAE1045 joint, the fractography is mainly composed of plastic-slipping plane and dimples (Fig. 8a), indicating that fracture of brazed joints is ductile fracture pattern, demonstrated by the stress-strain curves (Fig. 9). Figure 8(b) shows that the fractography of the WC-8Co/Ag-28Cu/SAE1045 joint is mainly dimples. Most of the residual thermal stresses in the brazed joints can be dissipated by the plastic deformation of the filler metals because of the excellent plasticity of the two brazing filler metals (Cu and Ag-28Cu alloy). As a result, the two joint fractures do not occur along the WC-8Co/interlayer interface or in the bulk WC-8Co substrate near the interlayer. The mean shear strength of WC-8Co/SAE1045 brazed joint using pure Cu as filler metal is 172 ± 8 MPa, while that of the brazed joint using the Ag-28Cu as filler metal is 136 ± 5 MPa, which is closely related to shear strength of the interlayers. Based on the XRD analysis (Fig. 8), the fracture surface of WC-8Co/Cu/SAE1045 joint is composed of Cu(Co,Fe) solid solution, while that of WC-8Co/Ag-28Cu/SAE1045 joint mainly consists of Ag(Cu) and Cu(Ag,Fe) solid solutions, indicating that both the joint fractures occur in the interlayers. It is noted that there are some displacements in Bragg diffraction angles of Ag and Cu, which should be attributed to the positioning of solute atoms leading to the lattice deformation of Cu and Ag atoms (Ref 27). The formation of solid solutions can be derived from the elemental diffusion of the SAE1045 steel and WC-8Co substrates into the filler metals.

4. Conclusions

The WC-8Co/SAE1045 steel joints were fabricated by vacuum brazing based on the wetting of molten Cu and Ag-28Cu alloy on the WC-8Co cemented carbide. For the Cu/WC-8Co wetting system, the equilibrium is obtained after ~ 10 min and the equilibrium contact angle decreases from 15° to 4° with the temperature increasing from 1090 to 1100 $^\circ\text{C}$. However, for the Ag-28Cu/WC-8Co wetting system, the spreading cannot reach the equilibrium after over 60 min and the final contact angle decreases from 37.2° to 24.3° with the temperature increasing from 830 to 850 $^\circ\text{C}$. A transition interlayer containing Fe, Co and Cu forms at the WC-Co/Cu interface in the

WC-8Co/Cu/SAE1045 brazed joint. The Co from the WC-8Co substrate can diffuse across the Cu or Ag-28Cu interlayer into the SAE1045 steel. Both the microhardness values in the WC-8Co substrate adjacent to the WC-8Co/interlayer interfaces obviously decrease compared to the original microhardness of the WC-8Co substrate. The variation of microhardness values in the SAE1045 substrate adjacent to the SAE1045/interlayer interfaces is mainly related to the diffusion level of Co into the two steel substrates. Both joint fractures occur in the Cu or Ag-28Cu interlayer, and ductile fracture is the main fracture mode. The mean shear strength values of WC-Co/Cu/SAE1045 and WC-Co/Ag-28Cu/SAE1045 brazed joints are about 172 and 136 MPa, respectively.

Acknowledgments

This work is supported by the National Natural Science Foundation of China (51572112), the Natural Science Foundation of Jiangsu Province (BK20151340), the Six Talent Peaks Project of Jiangsu Province (2014-XCL-002), the Postdoctoral Science Foundation of China (2014M551512), the Innovation/Entrepreneurship Program of Jiangsu Province ([2013]477 and [2015]26), the Qing Lan Project ([2016]15), and the Research and Innovation Project for College Graduates of Jiangsu Province (KYLX15_1058).

References

- H.O. Andren, Microstructures of Cemented Carbides, *Mater. Des.*, 2001, **22**(6), p 491–498
- K. Bonny, P. De Baets, Y. Perez, J. Vleugels, and B. Lauwers, Friction and Wear Characteristics of WC-Co Cemented Carbides in Dry Reciprocating Sliding Contact, *Wear*, 2010, **268**(11), p 1504–1517
- A.M. Soleimanpour, P. Abachi, and A. Simchi, Microstructure and Mechanical Properties of WC-10Co Cemented Carbide Containing VC or (Ta, Nb)C and Fracture Toughness Evaluation Using Different Models, *Int. J. Refract. Met. Hard. Mater.*, 2012, **31**, p 141–146
- A.H. Li, J. Zhao, D. Wang, X.L. Gao, and H.W. Tang, Three-Point Bending Fatigue Behavior of WC-Co Cemented Carbides, *Mater. Des.*, 2013, **45**, p 271–278
- T.T. Shen, D.H. Xiao, X.Q. Ou, M. Song, Y.H. He, N. Lin, and D.F. Zhang, Effects of LaB₆ Addition on the Microstructure and Mechanical Properties of Ultrafine Grained WC-10Co Alloys, *J. Alloys Compd.*, 2011, **509**(4), p 1236–1243
- H.S. Chen, K.Q. Feng, S.F. Wei, J. Xiong, Z.X. Guo, and H. Wang, Microstructure and Properties of WC-Co/3Cr13 Joints Brazed Using Ni Electroplated Interlayer, *Int. J. Refract. Met. Hard. Mater.*, 2012, **33**, p 70–74
- M. Uzkut, N.S. Sinan Koksall, and B.S. Unlu, The Determination of Element Diffusion in Connecting SAE 1040/WC Material by Brazing, *J. Mater. Process. Technol.*, 2005, **169**(3), p 409–413
- Q.Y. Zhai, C.K. Liang, J. Cheng, J.F. Xu, J.P. Liu, and Q.S. Xue, Vacuum Brazing of 25Cr3MoA/YG6 Using Cu-Based Microcrystalline Brazing Alloy, *Acta Metall. Sin.*, 2008, **44**, p 1136–1140
- S.A.A. Akbari Mousavi, P. Sherafati, and M.M. Hoseinion, Investigation on Wettability and Metallurgical and Mechanical Properties of Cemented Carbide and Steel Brazed Joint, *Adv. Mater. Res.*, 2012, **445**, p 759–764
- S. Yaoita, T. Watanabe, and T. Sasaki, Effects of Ni and Co Elements in Filler Metals in Ag Brazing of Cemented Carbide, *Mater. Res. Innov.*, 2013, **17**, p 142–147
- C. Jiang, H. Chen, Q.Y. Wang, and Y.X. Li, Effect of Brazing Temperature and Holding Time on Joint Properties of Induction Brazed WC-Co/Carbon Steel Using Ag-based Alloy, *J. Mater. Process. Technol.*, 2016, **229**, p 562–569
- W.B. Lee, B.D. Kwon, and S.B. Jung, Effect of Bonding Time on Joint Properties of Vacuum Brazed WC-Co Hard Metal/Carbon Steel Using

- Stacked Cu and Ni Alloy as Insert Metal, *Mater. Sci. Technol.*, 2004, **20**(11), p 1474–1478
13. W.B. Lee, B.D. Kwon, and S.B. Jung, Effects of Cr_3C_2 on the Microstructure and Mechanical Properties of the Brazed Joints Between WC-Co and Carbon Steel, *Int. J. Refract. Met. Hard Mater.*, 2006, **24**(3), p 215–221
 14. T. Iamboliev, S. Valkanov, and S. Atanasova, Microstructure Embrittlement of Hard Metal-Steel Joint Obtained under Induction Heating Diffusion Bonding, *Int. J. Refract. Met. Hard Mater.*, 2013, **37**, p 90–97
 15. K.Q. Feng, H.S. Chen, J. Xiong, and Z.X. Guo, Investigation on Diffusion Bonding of Functionally Graded WC-Co/Ni Composite and Stainless Steel, *Mater. Des.*, 2013, **46**, p 622–626
 16. M.I. Barrena, J.M. Gomez de Salazar, and L. Matesanz, Ni–Cu Alloy for Diffusion Bonding Cermet/Steel in Air, *Mater. Lett.*, 2009, **63**(24), p 2142–2145
 17. P.Q. Xu, J.W. Ren, P.L. Zhang, H.Y. Gong, and S.L. Yang, Analysis of Formation and Interfacial WC Dissolution Behavior of WC-Co/Invar Laser-TIG Welded Joints, *J. Mater. Eng. Perform.*, 2013, **22**(2), p 613–623
 18. D.R. Zhou, H.C. Cui, P.Q. Xu, and F.G. Lu, Tungsten Carbide Grain Size Computation for WC-Co Dissimilar Welds, *J. Mater. Eng. Perform.*, 2016, **25**(6), p 2500–2510
 19. Y.G. Guo, B.X. Gao, G.W. Liu, T.T. Zhou, and G.J. Qiao, Effect of Temperature on the Microstructure and Bonding Strength of Partial Transient Liquid Phase Bonded WC-Co/40Cr Joints Using Ti/Ni/Ti Interlayers, *Int. J. Refract. Met. Hard Mater.*, 2015, **51**, p 250–257
 20. P. Shen, X.H. Zheng, H.J. Liu, and Q.C. Jiang, Wetting of WC by a Zr-base Metallic Glass-Forming Alloy, *Mater. Chem. Phys.*, 2013, **139**(2), p 646–653
 21. Y.W. Zhao, Y.J. Wang, Y. Zhou, and P. Shen, Reactive Wetting and Infiltration of Polycrystalline WC by Molten Zr_2Cu Alloy, *Scr. Mater.*, 2011, **64**(3), p 229–232
 22. G.W. Liu, F. Valenza, M.L. Muolo, and A. Passerone, SiC/SiC and SiC/Kovar Joining by Ni–Si and Mo Interlayers, *J. Mater. Sci.*, 2010, **45**(16), p 4299–4307
 23. H. Baker, and H. Okamoto, *ASM Hand-Book, Volume 3 Alloy Phase Diagrams*, ASM International, The Materials Information Society, Materials Park, OH, 1992
 24. V. Raghvan, Co-Cu-Fe (Cobalt-Copper-Iron), *J. Phase Equilib. Diff.*, 2008, **29**(6), p 518–519
 25. C.P. Wang, X.J. Liu, I. Ohnuma, R. Kainuma, and K. Ishida, Phase Equilibria in Fe–Cu–X (X: Co, Cr, Si, V) Ternary Systems, *J. Phase Equilib.*, 2002, **23**(3), p 236–245
 26. M.I. Barrena, J.M. Gomez de Salazar, and L. Matesanz, Interfacial Microstructure and Mechanical Strength of WC-Co/90MnCrV8 Cold Work Tool Steel Diffusion Bonded Joint with Cu/Ni Electroplated Interlayer, *Mater. Des.*, 2010, **31**, p 3389–3394
 27. S.H. Hashemian Rahaghi, R. Poursalehi, and R. Miresmaeili, Optical Properties of Ag-Cu Alloy Nanoparticles Synthesized by DC Arc Discharge in Liquid, *Procedia Mater. Sci.*, 2015, **11**, p 738–742